PHOTONICS Research

Quantum dots assisted *in vivo* two-photon microscopy with NIR-II emission

Huwei Ni,[1,†] Yalun Wang,[2,†] Tao Tang,[3] Wenbin Yu,[1] Dongyu Li,[4] Mubin He,[1] Runze Chen,[1] Mingxi Zhang,[3,5] and Jun Qian[1,6]

[1]*State Key Laboratory of Modern Optical Instrumentations, Centre for Optical and Electromagnetic Research, College of Optical Science and Engineering, International Research Center for Advanced Photonics, Zhejiang University, Hangzhou 310058, China*
[2]*SIEE (Sussex AI Institute), Zhejiang Gongshang University, Hangzhou 310018, China*
[3]*State Key Laboratory of Advanced Technology for Materials Synthesis and Processing, Wuhan University of Technology, Wuhan 430070, China*
[4]*Britton Chance Center for Biomedical Photonics, Wuhan National Laboratory for Optoelectronics, Huazhong University of Science and Technology, Wuhan 430074, China*
[5]*e-mail: mxzhang@whut.edu.cn*
[6]*e-mail: qianjun@zju.edu.cn*

With the advantages of high resolution and deep penetration depth, two-photon excited NIR-II (900–1880 nm) fluorescence (2PF) microscopic bioimaging is promising. However, due to the lack of imaging systems and suitable probes, few such works, to our best knowledge, were demonstrated utilizing NIR-II excitation and NIR-II fluorescence simultaneously. Herein, we used aqueously dispersible PbS/CdS quantum dots with bright NIR-II fluorescence as the contrast agents. Under the excitation of a 1550 nm femtosecond (fs) laser, they emitted bright 2PF in the NIR-II region. Moreover, a 2PF lifetime imaging microscopic (2PFLIM) system was implemented, and *in vivo* 2PFLIM images of mouse brain blood vessels were obtained for the first time to our best knowledge. To improve imaging speed, an *in vivo* two-photon fluorescence microscopy (2PFM) system based on an InGaAs camera was implemented, and *in vivo* 2PFM images of QDs-stained mouse brain blood vessels were obtained.   © 2021 Chinese Laser Press

https://doi.org/10.1364/PRJ.441471

1. INTRODUCTION

Bioimaging is an indispensable method in medical research, clinical diagnosis, and treatment. Various biological imaging technologies are widely used, such as magnetic resonance imaging (MRI), computed tomography (CT), and Doppler ultrasonography. Nevertheless, due to the limited spatial resolution or biological damage caused by ionizing radiation, their application is constrained. With the virtue of high resolution, fast response, and good biocompatibility, fluorescence imaging is a promising alternative [1,2]. Due to the attenuation of light in biological tissues, the depth of fluorescence imaging is limited (<1 mm). To improve effective imaging depth, light in the second near-infrared (NIR-II, 900–1880 nm) optical transparence window for biological tissues is utilized, as it is scattered less than light in the visible or first near-infrared (NIR-I, ~700–900 nm) window [3–12]. Recently, many works about the NIR-II region have been reported [13–15], and the imaging depth has been apparently improved. As most of them describe only NIR-II excitation or NIR-II emission, the potential of the NIR-II region for optical bioimaging can be further developed.

As a powerful tool to explore biological structures and functions, two-photon fluorescence (2PF) imaging is widely used [16–18]. In a 2PF process, the fluorophore simultaneously absorbs two photons with low energy and emits a single photon with high energy. Besides, as a third-order nonlinear optical process, 2PF is confined to the focus, thus increasing the signal-to-background ratio (SBR). There are a lot of works on 2PF imaging, while most of them concentrate on the 2PF signals in the visible light region. Considering the effective attenuation length of light in the NIR-II region [7], the exploration of 2PF in the NIR-II region would be promising.

The exploration of 2PF imaging in the NIR-II region would suffer from the lack of appropriate probes. Most of the fluorophores exhibit small absorption cross-section and low quantum yield efficiency in the NIR-II region, and the emission would be faint. As an alternative, PbS QDs have strong and tunable emission covering the NIR-II region [19–21] and would be a

promising candidate. Based on this, a kind of novel aqueously dispersible core/shell lead sulfide (PbS)/cadmium sulfide (CdS) QDs was synthesized, with good photochemical stability and biocompatibility [21]. Thus, with the help of PbS/CdS QDs, 2PF imaging in the NIR-II region could be anticipated.

To enhance the detection of weak fluorescence, time-correlated single-photon counting (TCSPC) technology was introduced [22,23]. It measures the fluorescence lifetime, and the noise can be greatly reduced by filtering [24]. Combined with multiphoton fluorescence microscopy (MPFM), multiphoton fluorescence lifetime imaging microscopy (MPFLIM) is obtained and able to capture weak signals. Compared with traditional fluorescence intensity-based microscopic imaging methods, MPFLIM imaging can provide more precise imaging on weak signals, and it would be more suitable to detect weak 2PF signals in the NIR-II region. In addition, due to the small detection area of commonly used detectors (e.g., InGaAs photomultiplier tube) in the NIR-II region, an infrared (900–1700 nm) sensitive InGaAs camera with large detection area and high quantum efficiency can also be adopted as the detector in the MPFM system.

In this work, the chemical and optical properties of aqueously dispersible PbS/CdS QDs were studied. Under the 1550 nm fs laser excitation, PbS/CdS QDs emit fluorescence in the NIR-II region, centered at 1270 nm. The power-dependence relationship was further studied, and the 2PF process was verified. Furthermore, PbS/CdS QDs were utilized for *in vivo* 2PF cerebral vasculature imaging in a mouse brain. With a photomultiplier tube (PMT) as the detector, a 2PFM system with a TCSPC module was built. For the first time, 2PF lifetime microscopy (2PFLIM) with excitation and emission in the NIR-II region was obtained, with a penetration depth of 220 μm and good contrast. Furthermore, to improve the fluorescence collection efficiency, an InGaAs camera was introduced to take the place of PMT in the 2PFLIM system. In this case, imaging speed was significantly improved, out-of-focus fluorescence suppression effect could be observed directly, and through-skull 2PF imaging of brain blood vessels with a penetration depth of 110 μm was obtained. This work shows the

possibility of two-photon microscopy with excitation and emission in the NIR-II region for biological imaging applications.

2. EXPERIMENT

One-photon fluorescence (1PF) and 2PF spectra of QDs were measured by a homemade spectral measurement system. The QDs solution was placed into a quartz cuvette with transparent walls. The excitation light, whose parameters were dependent on the requirement of spectrum measurement [in this work, a continuous wave (CW) laser (MXL-III-665, CNI, China)] with a center wavelength of 665 nm was for 1PF, and a femtosecond laser (FLCPA-01C, Calmar Laser, 400 fs, 1 MHz) with a center wavelength of 1550 nm was for 2PF and focused through a lens. To reduce the self-absorption of the solution, the focus was adjusted as close to the inner surface of the cuvette as possible. Then, the fluorescence signals were collected by an objective (XLPLN25XWMP2, Olympus, 25×, working distance = 2.0 mm, NA = 1.05) in the perpendicular direction of the incident light. The fluorescence signals were recorded by a spectrometer (NIR-2500, Ideaoptics Instruments, China). The relationship of 1550 nm femtosecond excitation power and fluorescence intensity from QDs was obtained by the same spectral measurement system. For a nonlinear process based on multiphoton excitation, $FL = P^k$ (FL represents the fluorescence intensity; P represents the power of the laser; k represents the order); $\lg FL = k \cdot \lg P$ is obtained through logarithmic transformation. By measuring the fluorescence intensity at different powers, the k value can be calculated.

The 2PFLIM system (Fig. 1) in the NIR-II region was composed of a scanning microscope (FV1200 & BX61, Olympus), a TCSPC board card (SPC-150, Becker & Hickl GmbH), and a NIR PMT (H12397-75, Hamamatsu), under 1550 nm fs laser excitation. The beam whose polarization state has been adjusted by the half-wave plate was divided into two vertical directions by the polarization beam splitter (PBS) and used as excitation light and synchronization signal, respectively. The excitation light was introduced into a scanning microscope (FV1200&BX61, Olympus), reflected by a 1500 nm short-pass dichroic mirror (DM) and focused at different depths
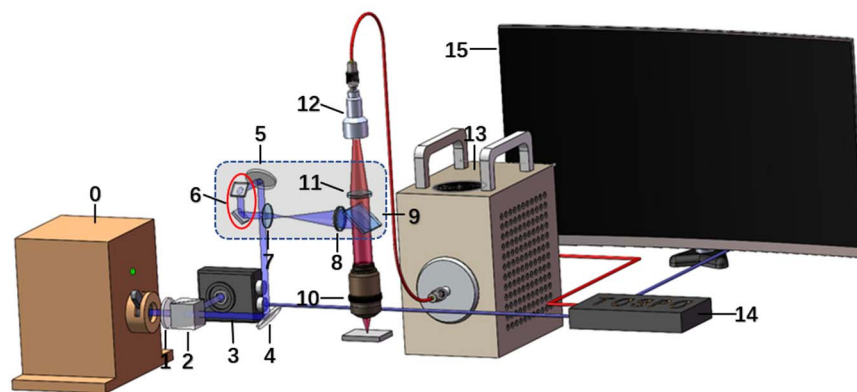

Fig. 1. Schematic illustration of 2PFLIM system (PMT as the detector) in the NIR-II region. 0) 1550 nm fs laser; 1) half-wave plate; 2) polarization beam splitter (PBS); 3) photodiode; 4,5) reflector; 6) scanning galvanometer; 7,8,11) lens; 9) dichroic mirror; 10) objective; 12) large beam collimator; 13) PMT; 14) TCSPC board; 15) computer. Dashed box is the scanning microscope.

of the sample through a *Z*-axis adjustable objective (XLPLN25XWMP2, Olympus, 25×, working distance = 2.0 mm, NA = 1.05) to excite fluorescence. The fluorescence signal collected by the same objective passed through the aforementioned DM, and it was coupled into the optical fiber by the tube lens and large beam collimator. Finally, the fluorescence signal was captured by the PMT. According to the fluorescence signal and the synchronization signal, the fluorescence lifetime microscopic image was obtained by the TCSPC board.

The 2PFM system in the NIR-II region was similar to the 2PFLIM system, while the signal-collection module replaced by the InGaAs camera (SD640, Tekwin, China) was greatly simplified.

3. RESULTS AND DISCUSSION

A. Characterization of QDs

Aqueously dispersible PbS/CdS QDs were synthesized according to our previously reported work [21]. Quantum yield ($QY_{QDs} = 17.6\%$ in H_2O) and two-photon absorption cross-section ($\sigma_{QDs,2P,1550} = 530$ GM in H_2O) of QDs were measured by using a standard organic dye ICG as reference [25–27]. The fluorescence lifetime ($\tau = 501$ ns in H_2O) of PbS/CdS QDs was measured by the home-built 2PFLIM system (Fig. 1). The morphology of PbS/CdS QDs was characterized by transmission electron microscopy (TEM) and dynamic light scattering (DLS). The TEM image revealed that PbS/CdS QDs were well dispersed, with a spherical shape

[Fig. 2(a)]. The DLS profile showed that the average size of QDs was about 32.34 nm [Fig. 2(b)], which was proper for bioimaging. Figure 2(c) shows the 1PF and 2PF spectra of PbS/CdS QDs. A 1300 nm short-pass filter was used to filter out the 1550 nm fs laser in the measurement, and only part of the 2PF spectrum was recorded. The 1PF and 2PF emissions of PbS/CdS QDs were in the NIR-II region, centered at 1276 and 1270 nm, respectively, with full width at half maximum of about 200 nm. The power-dependence relationship is shown in Fig. 2(d). The logarithm of the fluorescence intensity of PbS/CdS QDs had good linear proportion to the logarithm of the excitation power, with a slope of 1.72, which was close to 2. It indicated that near-infrared anti-Stokes photoluminescence from PbS QDs has taken place [28], but 2PF was dominant.

B. PMT-Based 2PFLIM Imaging in the NIR-II Region

In vivo 2PFLIM was further conducted. Aqueously dispersible PbS/CdS QDs centered at 1270 nm were used as probes to label mouse brain vessels via intravenous injection. An eight-week-old male mouse with craniotomy was anesthetized and then intravenously injected with 200 μL aqueous QDs (2 mg/mL, PBS, 1×). The brain vessels were imaged by the aforementioned 2PFLIM imaging system (Fig. 1) equipped with a 1550 nm fs laser as excitation. Under the condition of an integration time of 40 s per frame, the 2PFLIM images of cerebral vasculatures and fluorescence lifetime information of various vertical depths (from 0 to 220 μm) were obtained (Fig. 3). Cerebral blood vessels at various depths were clearly
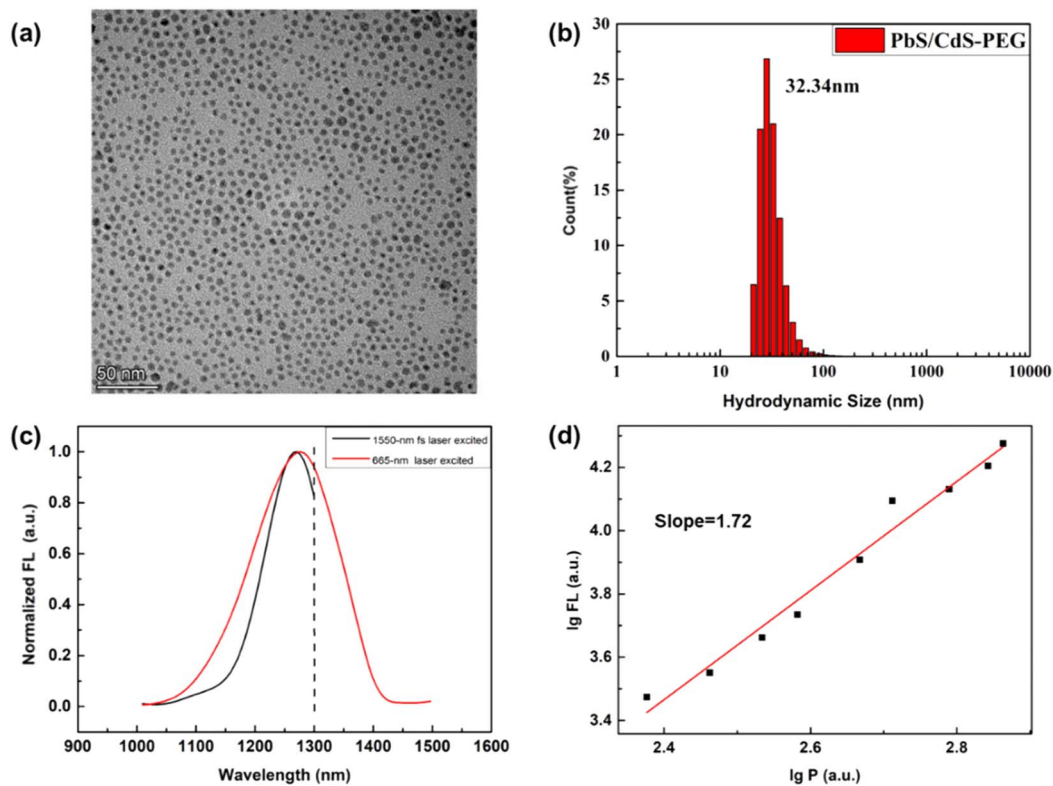

Fig. 2. Morphological characterization and optical properties of PbS/CdS quantum dots (PbS QDs). (a) Transmission electron microscopy (TEM) image of PbS QDs. (b) Dynamic light scattering (DLS) profile of PbS QDs. (c) One-photon and multiphoton fluorescence spectra of PbS QDs. (d) Relationship of 1550 nm fs excitation power and fluorescence intensity from QDs.

visible [Figs. 3(f)–3(i)], and small blood vessels could be easily distinguished with the help of fluorescence lifetime information [Fig. 3(d)]. In addition, the NIR-II fluorescence lifetime of each position was obtained at the same time [Figs. 3(c) and 3(e)]. The fluorescence lifetimes are 520 ns (at 60 μm) and 300 ns (at 220 μm), respectively. Due to the low overall photon counts, a difference of 320 ns was found in lifetime, while they should be the same in theory. For weak signals, the signal intensity can be enhanced by long time integration in TCSPC, while it is still difficult to accurately obtain the lifetime values. Although some vessels can be seen within the 220 μm penetration depth in our built 2PFLIM imaging system, deeper penetration depth is of great need in *in vivo* imaging. Besides, in

most multiphoton fluorescence microscopes, a penetration depth of 400 μm could be obtained. Currently, compared with visible/NIR-I PMT (H7422-40/50, $\varphi = 5$ mm, $\eta > 10\%$), the detection area and quantum efficiency of InGaAs PMT (H12397-75, $\varphi = 1.6$ mm, $\eta < 2\%$) are much smaller, which causes such detectors to rely on optical fibers to collect fluorescence. In the process of coupling, most parts of the fluorescence were lost (more than 50%). Therefore, the performance of the imaging system, mainly limited by the immature NIR-II detector, is not good enough to meet the needs of *in vivo* imaging and is inferior to ordinary multiphoton fluorescence imaging whose fluorescence is in the visible region and the excitation light is in the near-infrared region.
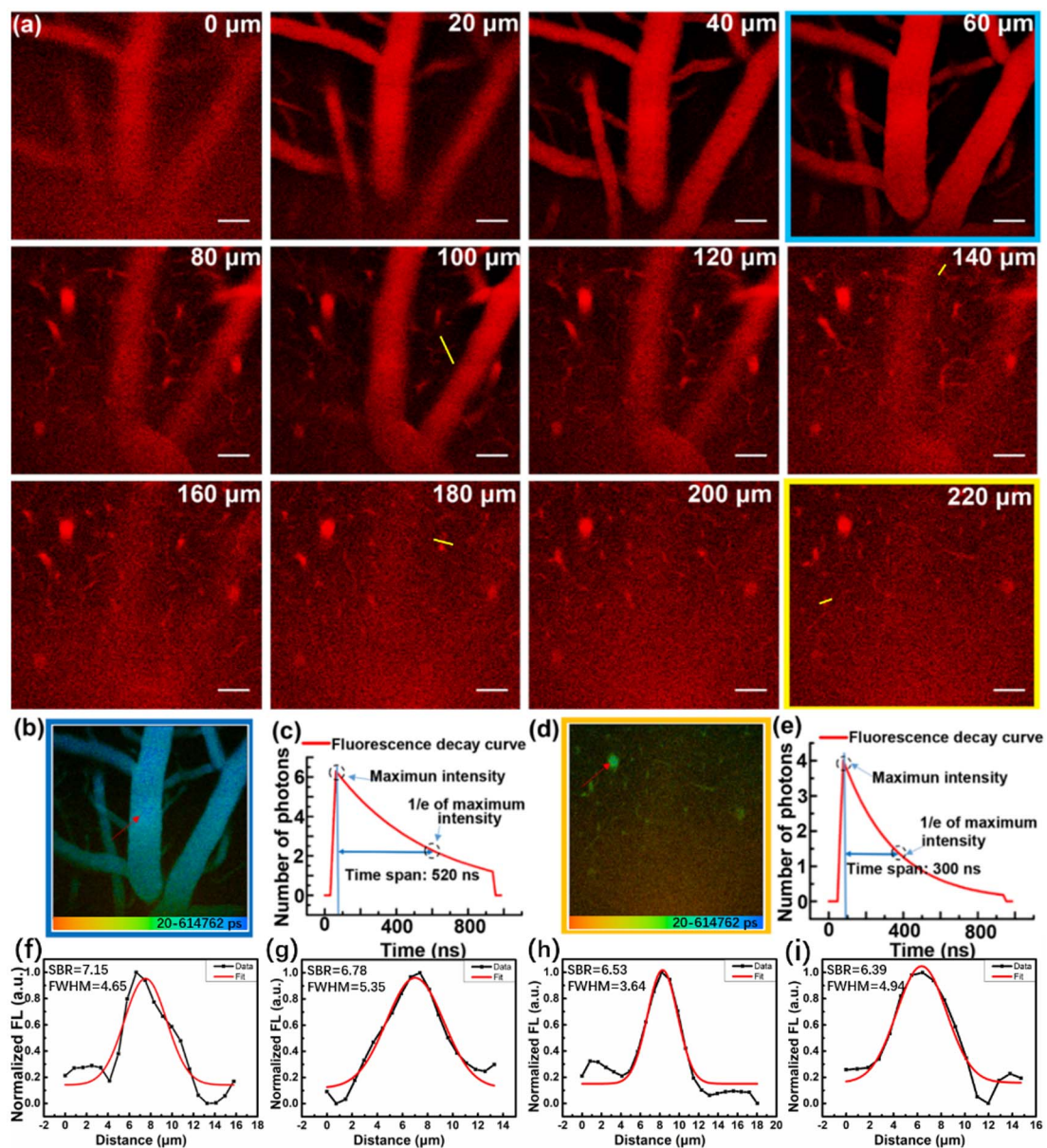

Fig. 3. *In vivo* 2PFLIM images of QDs-stained mouse brain blood vessels with PMT. (a) 2PF intensity images of brain blood vessels at different vertical penetration depths: from 0 to 220 μm. Scale bar: 50 μm. (b) 2PF lifetime image at 60 μm. (c) Time-resolved decay curve at the arrow in (b). (d) 2PFLIM image at 220 μm. (e) Time-resolved decay curve at the arrow in (d). (f)–(i) Plots of each FWHM of blood vessels at depth of 100, 140, 180, and 220 μm, as indicated by the yellow lines in (a), respectively.

C. InGaAs Camera-Based 2PFM Imaging in the NIR-II Region

From the perspective of increasing the area of the detector, an InGaAs camera was chosen as the detector for 2PFM. Both of the excitation and emission are in the NIR-II region, which can minimize the scattering of light by biological tissues [29]. Real information can be obtained with little distortion by camera detection, which has been confirmed by wide-field microscopic imaging works in the NIR-II region [30,31]. This means the NIR-II fluorescence signal on the focus can reach the camera's detection area without much aberration (mainly caused by tissue scattering), and each point of the sample corresponds to a pixel of the camera. Each pixel is working until the laser has scanned all points; further, the information of each pixel forms a complete image eventually. Besides, it is not necessary to perform a complex image program to reconstruct the fluorescence image *in vivo*.

Because TCSPC is not applicable in fast bioimaging, an InGaAs camera with large detection area (16 mm × 12.8 mm) and high quantum efficiency ($\eta = \sim 70\%$) was used. The 2PFM system in the NIR-II region was further realized by using an InGaAs camera as a detector instead of PMT [Fig. 4(a)]. The excitation light path was basically the same; however, the components related to the synchronization signal were removed. Besides, the fluorescence was focused on the InGaAs

camera via a tube lens, avoiding losses in the coupling process. Ultimately, a 2PFM image was obtained by camera image.

A flat cuvette filled with aqueous dispersion of QDs was placed under the objective, and the fluorescence images were obtained when laser was focused at different depths by adjusting the Z axis of the objective [Fig. 4(b)]. The area of the fluorescence spot at each depth was measured [Fig. 4(c)]. This confirmed that fluorescence was only excited at the focal point. Due to the absorption of water, the laser power density and fluorescence spot area decreased as the depth increased when incident light power remained constant, which meant only the central area with higher power density than threshold produced fluorescence, and the fluorescence from QDs under 1550 nm fs laser excitation was mainly multiphoton fluorescence. In addition, water also has some absorption on NIR-II fluorescence; it removes the scattered fluorescence signals and reduces the side lobes of fluorescence.

The cranial window may cause inflammation and damage to the brain and affect its functional structure [32]. Therefore, skull optical clearing was used in 2PFM imaging to reduce optical scattering caused by skull and biological damage, when fluorescence collection efficiency was improved significantly by the InGaAs camera. An eight-week-old male mouse with skull optical clearing window was anesthetized and then intravenously injected with 200 μL aqueous dispersion of QDs
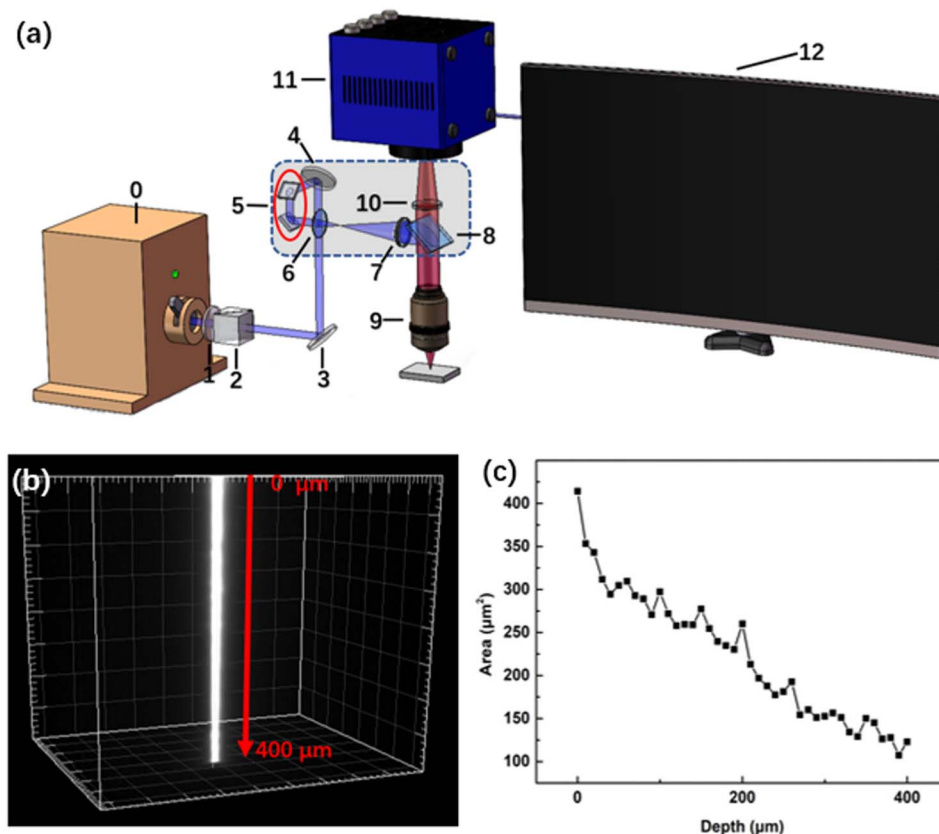

Fig. 4. (a) Schematic illustration of 2PFM system (InGaAs camera as the detector) in the NIR-II region. 0) 1550 nm fs laser; 1) half-wave plate; 2) polarization beam splitter (PBS); 3,4) reflector; 5) scanning galvanometer; 6,7,10) lens; 8) dichroic mirror; 9) objective; 11) InGaAs camera; 12) computer. Dashed box is the scanning microscope. (b) 3D reconstructed image of fluorescence spots when laser is focused at different depths. (c) Statistics of fluorescence area at various depths.
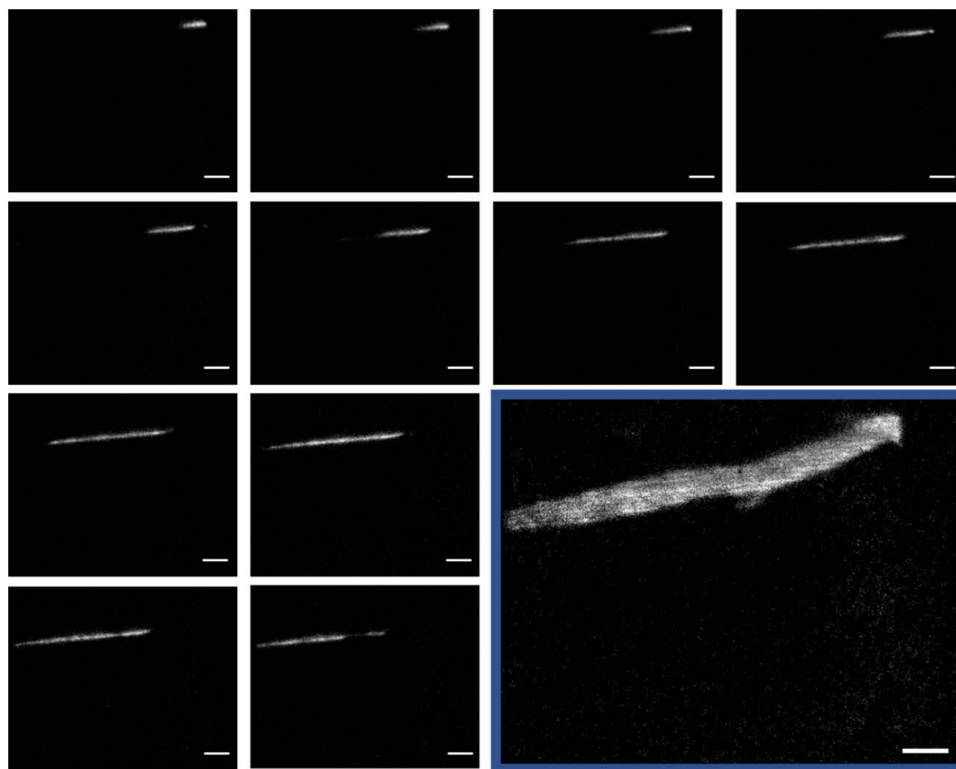
Fig. 5.   Schematic diagram of image overlay: the blood vessel image in the blue box is superimposed by the other 15 frames. Scale bar: 50 μm.

(2 mg/mL, PBS, 1X) [33]. The cerebral vasculatures were imaged by the 2PFM system [Fig. 4(a)] equipped with a 1550 nm fs laser. Due to limitations of exposure time (50 ms) of the camera, about 50 frames of the camera's images were directly superimposed to obtain a complete 2PFM image, and the temporal resolution of each frame was ~0.4 Hz. As shown in the

diagram, a local blood vessel image in the blue box was superimposed by the other 15 frames (Fig. 5).

At a scanning speed of 10 μs/pixel, 2PFM images of cerebral vasculatures, via skull optical clearing process, at various vertical depths (from 0 to 110 μm) were obtained [Fig. 6(a)]. The whole process of the appearance and disappearance of blood
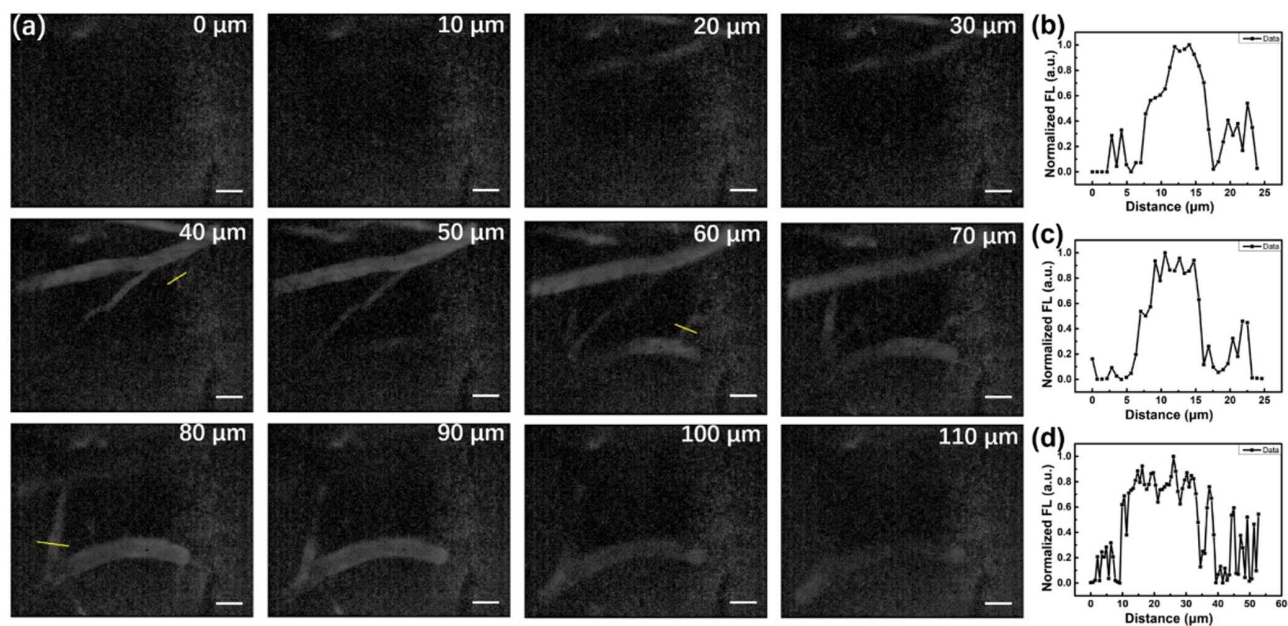

Fig. 6.   *In vivo* 2PFM images of QDs-stained mouse brain blood vessels with InGaAs camera. (a) 2PFM images of brain blood vessels at different vertical penetration depths: from 0 to 110 μm. Scale bar: 50 μm. (b)–(d) Plots of each FWHM of blood vessels at depths of 40, 60, and 80 μm as indicated by the yellow lines in (a), respectively.

vessels in different layers could be observed clearly, confirming that InGaAs cameras with large detection areas can be used for 2PF microscopy imaging. The InGaAs camera with high quantum efficiency solves the problem of fluorescence collection. However, the raw data [Figs. 6(b)–6(d)] are not smooth, and the noise of InGaAs camera caused by dark current cannot be ignored. A lot of noise accumulates during the imaging process, which makes it impossible to detect deep information and images of small blood vessels. This problem may be solved by using high-performance InGaAs cameras with deep cooling to suppress noise as much as possible.

4. CONCLUSIONS AND OUTLOOK

In summary, aqueously dispersible PbS/CdS QDs with bright NIR-II fluorescence, good photochemical stability, and biocompatibility were obtained. Moreover, NIR-II 2PFLIM was achieved with TCSPC, NIR-II PMT, and a scanning microscope for the first time. Due to low fluorescence collection efficiency, its time resolution was not high (40 s per frame). For the low scattering of NIR-II light in biological tissues, the NIR-II fluorescence signal will not be distorted after passing through the biological tissue, and an InGaAs camera could replace PMT for big detection areas and high quantum efficiency. To improve time resolution, an InGaAs camera was introduced as the detector, and the fluorescence signal was collected directly without the guidance of optical fibers in point-scanning multiphoton microscopy for the first time. This means fluorescence microscopy in the NIR-II region with the method of point-scanning and area-detecting is feasible due to the less scattering of NIR-II fluorescence. Compared with temporal focusing multiphoton microscopy in the NIR-II region [34], 2PFM with the InGaAs camera is able to reduce the requirement of pulse power, when NIR-II probes rely on a certain degree of excitation power. It can be anticipated that the InGaAs camera can directly obtain a complete NIR-II region fluorescence image during point-scanning without restructuring, when the integration time is long enough, the noise is relatively small, and the scanning speed is fast enough.

Disclosures. The authors declare no competing financial interests.

†These authors contributed equally to this paper.

REFERENCES

1. N. Ji, J. Freeman, and S. L. Smith, "Technologies for imaging neural activity in large volumes," Nat. Neurosci. **19**, 1154–1164 (2016).
2. X. Fan, Q. Xia, Y. Zhang, Y. Li, Z. Feng, J. Zhou, J. Qi, B. Tang, J. Qian, and H. Lin, "Aggregation-induced emission (AIE) nanoparticles-assisted NIR-II fluorescence imaging-guided diagnosis and surgery for inflammatory bowel disease (IBD)," Adv. Healthcare. Mater. 2101043 (2021).
3. Z. Feng, T. Tang, T. Wu, X. Yu, Y. Zhang, M. Wang, J. Zheng, Y. Yun, S. Chen, J. Zhou, X. Fan, S. Li, M. Zhang, and J. Qian, "Perfecting and extending the near-infrared biological window," Light Sci. Appl. **10**, 197 (2021).
4. H. Yang, R. Li, Y. Zhang, M. Yu, Z. Wang, X. Liu, W. You, D. Tu, Z. Sun, R. Zhang, X. Chen, and Q. Wang, "Colloidal alloyed quantum dots with enhanced photoluminescence quantum yield in the NIR-II window," J. Am. Chem. Soc. **143**, 2601–2607 (2021).
5. Q. Zhang, P. Yu, Y. Fan, C. Sun, H. He, X. Liu, L. Lu, M. Zhao, H. Zhang, and F. Zhang, "Bright and stable NIR-II J-aggregated AIE dibodipy-based fluorescent probe for dynamic *in vivo* bioimaging," Angew. Chem. **60**, 3967–3973 (2021).
6. X. Yu, Z. Feng, Z. Cai, M. Jiang, D. Xue, L. Zhu, Y. Zhang, J. Liu, B. Que, W. Yang, W. Xi, D. Zhang, J. Qian, and G. Li, "Deciphering of cerebrovasculatures via ICG-assisted NIR-II fluorescence microscopy," J. Mater. Chem. B **7**, 6623–6629 (2019).
7. L. A. Sordillo, Y. Pu, S. Pratavieira, Y. Budansky, and R. R. Alfano, "Deep optical imaging of tissue using the second and third near-infrared spectral windows," J. Biomed. Opt. **19**, 056004 (2014).
8. S. Golovynskyi, L. Golovynska, L. I. Stepanova, O. I. Datsenko, L. Liu, J. Qu, and T. Y. Ohulchanskyy, "Optical windows for head tissues in near-infrared and short-wave infrared regions: approaching transcranial light applications," J. Biophoton. **11**, e201800141 (2018).
9. A. M. Smith, M. C. Mancini, and S. M. Nie, "Bioimaging: second window for in vivo imaging," Nat. Nanotechnol. **4**, 710–711 (2009).
10. F. Helmchen and W. Denk, "Deep tissue two-photon microscopy," Nat. Methods **2**, 932–940 (2005).
11. A. N. Bashkatov, E. A. Genina, V. I. Kochubey, and V. V. Tuchin, "Optical properties of human skin, subcutaneous and mucous tissues in the wavelength range from 400 to 2000 nm," J. Phys. D **38**, 2543–2555 (2005).
12. M. Wang, C. Wu, D. Sinefeld, B. Li, F. Xia, and C. Xu, "Comparing the effective attenuation lengths for long wavelength *in vivo* imaging of the mouse brain," Biomed. Opt. Express **9**, 3534–3543 (2018).
13. Z. Feng, S. Bai, J. Qi, C. Sun, Y. Zhang, H. Ni, D. Wu, X. Fan, D. Xue, S. Liu, M. Chen, J. Gong, P. Wei, M. He, J. K. Y. Jacky, X. Li, B. Tang, L. Gao, and J. Qian, "Biologically excretable AIE dots for visualizing through the marmosets intravitally: horizons in future clinical nanomedicine," Adv. Mater. **33**, 2008123 (2021).
14. W. Liu, Y. Zhang, J. Qi, J. Qian, and B. Tang, "NIR-II excitation and NIR-I emission based two-photon fluorescence lifetime microscopic imaging using aggregation-induced emission dots," Chem. Res. Chin. U **37**, 171–176 (2021).
15. N. Alifu, A. Zebibula, H. Zhang, H. Ni, L. Zhu, W. Xi, Y. Wang, X. Zhang, C. Wu, and J. Qian, "NIR-IIb excitable bright polymer dots with deep-red emission for in vivo through-skull three-photon fluorescence bioimaging," Nano Res. **13**, 2632–2640 (2020).
16. Y. Li, Y. Sun, J. Li, Q. Su, W. Yuan, Y. Dai, C. Han, Q. Wang, W. Feng, and F. Li, "Ultrasensitive near-infrared fluorescence-enhanced probe for *in vivo* nitroreductase imaging," J. Am. Chem. Soc. **137**, 6407–6416 (2015).
17. K. Wang, A. Majewska, J. Schummers, B. Farley, C. Hu, M. Sur, and S. Tonegawa, "*In vivo* two-photon imaging reveals a role of arc in enhancing orientation specificity in visual cortex," Cell **126**, 389–402 (2006).
18. E. Garmire, "Nonlinear optics in daily life," Opt. Express **21**, 30532–30544 (2013).
19. K. D. Wegner and N. Hildebrandt, "Quantum dots: bright and versatile *in vitro* and *in vivo* fluorescence imaging biosensors," Chem. Soc. Rev. **44**, 4792–4832 (2015).
20. X. Shi, S. Chen, M. Luo, B. Huang, G. Zhang, R. Cui, and M. Zhang, "Zn-doping enhances the photoluminescence and stability of PbS quantum dots for *in vivo* high-resolution imaging in the NIR-II window," Nano Res. **13**, 2239–2245 (2020).
21. M. Zhang, J. Yue, R. Cui, Z. Ma, H. Wan, F. Wang, S. Zhu, Y. Zhou, Y. Kuang, Y. Zhong, D. Pang, and H. Dai, "Bright quantum dots emitting at similar to 1,600 nm in the NIR-IIb window for deep tissue fluorescence imaging," Proc. Natl. Acad. Sci. USA **115**, 6590–6595 (2018).
22. M. Y. Berezin and S. Achilefu, "Fluorescence lifetime measurements and biological imaging," Chem. Rev. **110**, 2641–2684 (2010).

23. L. Shang, N. Azadfar, F. Stockmar, W. Send, V. Trouillet, M. Bruns, D. Gerthsen, and G. U. Nienhaus, "One-pot synthesis of near-infrared fluorescent gold clusters for cellular fluorescence lifetime imaging," Small **7**, 2614–2620 (2011).

24. W. Becker, A. Bergmann, C. Biskup, L. Kelbauskas, T. Zimmer, N. Klocker, and K. Benndorf, "High resolution TCSPC lifetime imaging," Proc. SPIE **4963**, 175–184 (2003).

25. L. Cheng, K. Wang, and C. Xu, "Measurements of two-, three-, and four-photon excitation action cross sections," in *CLEO* (OSA, 2014), paper ATh3P.4.

26. M. Y. Berezin, C. Zhan, H. Lee, C. Joo, W. J. Akers, S. Yazdanfar, and S. Achilefu, "Two-photon optical properties of near-infrared dyes at 1.55 µm excitation," J. Phys. Chem. B **115**, 11530–11535 (2011).

27. Z. Feng, X. Yu, M. Jiang, L. Zhu, Y. Zhang, W. Yamg, W. Xi, G. Li, and J. Qian, "Excretable IR-820 for *in vivo* NIR-II fluorescence cerebrovascular imaging and photothermal therapy of subcutaneous tumor," Theranostics **9**, 5706–5719 (2019).

28. Y. Xiong, C. Liu, J. Wang, J. Han, and X. Zhao, "Near-infrared anti-Stokes photoluminescence of PbS QDs embedded in glasses," Opt. Express **25**, 6874–6882 (2017).

29. T. Wang and C. Xu, "Three-photon neuronal imaging in deep mouse brain," Optica **7**, 947–960 (2020).

30. X. Yu, Y. Ying, Z. Feng, J. Qi, J. Zheng, Y. Zhang, J. Liu, J. Qian, B. Tang, and D. Zhang, "Aggregation-induced emission dots assisted non-invasive fluorescence hysterography in near-infrared IIb window," Nano Today **39**, 101235 (2021).

31. X. Fan, Y. Li, Z. Feng, G. Chen, J. Zhou, M. He, L. Wu, S. Li, J. Qian, and H. Lin, "Nanoprobes-assisted multi-channel NIR-II fluorescence imaging-guided resection and photothermal ablation of lymph nodes," Adv. Sci. **8**, 2003972 (2021).

32. J. Wang, Y. Zhang, P. Li, Q. Luo, and D. Zhu, "Review: tissue optical clearing window for blood flow monitoring," IEEE J. Sel. Top. Quantum Electron. **20**, 6801112 (2014).

33. C. Zhang, W. Feng, Y. Zhao, T. Yu, P. Li, T. Xu, Q. Luo, and D. Zhu, "A large, switchable optical clearing skull window for cerebrovascular imaging," Theranostics **8**, 2696–2708 (2018).

34. C. J. Rowlands, O. T. Bruns, D. Franke, D. Fukamura, R. K. Jain, M. G. Bawendi, and P. T. C. So, "Increasing the penetration depth of temporal focusing multiphoton microscopy for neurobiological applications," J. Phys. D **52**, 264001 (2019).